

## Supporting information

### **Cost-effective and environmentally-friendly synthesis of 3D Ni<sub>2</sub>P from scrap nickel for highly efficient hydrogen evolution in both acidic and alkaline media**

*Yao Lin, Liangbo He, Tao Chen, Dan Zhou, Li Wu, Xiandeng Hou, and Chengbin Zheng\**

*\*Email: abinscu@scu.edu.cn*

**Reagents and materials:** Nickel chloride ( $\text{NiCl}_2 \cdot 6\text{H}_2\text{O}$ , 97%), formic acid (88%) and ethanol (95%) were all purchased from Kelong Chemical Reagent Co. Ltd. (Chengdu, China). Sodium hypophosphite ( $\text{NaH}_2\text{PO}_4$ ) and platinum on carbon (1 wt. % Pt/C, Pt on an activated carbon support) were purchased from Sigma-Aldrich. All chemicals were used as received without further purification. Deionized water (DIW, 18 M $\Omega$  cm) used in all experiments was purified by passage through an ultrapure purification system (Chengdu Ultrapure Technology Co., China). High purity Ar was obtained from Qiaoyuan Gas Co. (Chengdu, China). The PVG setup includes a peristaltic pump (BT100-02, Baoding Qili Precision Pump Co., Ltd.), a UV photochemical reactor consisting of a coiled quartz tube (60 cm length  $\times$  2.0 mm i.d.  $\times$  3.0 mm o.d.) wrapped around a 15 W low pressure mercury vapor UV lamp, and a quartz gas liquid phase separator (GLS). A homemade quartz tube (80 mm length  $\times$  10 mm i.d.  $\times$  13 mm o.d.) with tightly wrapped in a polyimide heating film (60 mm length  $\times$  34 mm wide), which was used as a miniaturized chemical vapor deposition (CVD) reactor.

## Electrochemical calculation

**1. Catalyst loading.** To calculate the mass of  $\text{Ni}_2\text{P}$  nanoparticles grown on the carbon cloth, the change in weight of the carbon cloth ( $m_1$ , mg) could be directly measured.<sup>[1]</sup>  $m_{\text{Ni}_2\text{P}} = m_1 \times (M_{\text{Ni}_2\text{P}} / M_{\text{P}}) = m_1 \times (149/31) = 4.8 m_1$  mg, where  $M_{\text{Ni}_2\text{P}}$  and  $M_{\text{P}}$  are the molecular weight of  $\text{Ni}_2\text{P}$  and atomic weight of P, respectively. The average of the weight increases ( $m_1$ ) in our case was 0.563 mg. The  $\text{Ni}_2\text{P}$  NPs/CC electrodes were sealed for the working surface area ( $a=0.25$  cm<sup>2</sup>). So the loaded density of  $\text{Ni}_2\text{P}$  nanoparticles was  $m_{\text{Ni}_2\text{P}}/a = 10.8$  mg cm<sup>-2</sup>.

**2. Potential referencing between different electrodes.** When a SCE served as the reference electrode, potential was referenced to the RHE through the relationship  $E$  (vs. RHE) =  $E$  (vs. SCE) + 0.270 V + 0.05916  $\times$  pH. When the reference electrode was replaced by a Hg/HgO electrode with the inner reference electrolyte of 1 M KOH, potential were referenced to the RHE through the relationship  $E$  (vs. RHE) =  $E$  (vs. Hg/HgO) + 0.0977 V + 0.05916  $\times$  pH.

**3. Tafel slope.** Polarization curves were replotted as overpotential ( $\eta$ ) versus log current density ( $\log j/[j]$ ) to get Tafel plots. By fitting the linear portion of the Tafel

plots to the Tafel equation ( $\eta = b \log j/[j] + a$ ), the Tafel slope ( $b$ ) was obtained.

**4. Calculation of electrochemically active surface area.** The calculation of electrochemically active surface area (ECAS) is based on the measured double layer capacitance of the NiO and Ni<sub>2</sub>P NPs/CC in 0.5 M H<sub>2</sub>SO<sub>4</sub> and 1 M KOH. Briefly, a series of CVs was performed across 0.31 V~0.41 V and -0.95 V~-0.85 V in 0.5 M H<sub>2</sub>SO<sub>4</sub> and 1 M KOH at scan rates of 40, 80, 120, 160 and 200 mV/s. The slope of the charging current ( $i_c$ ) as a function of the scan rate ( $v$ ) gives a straight line of slope equal to the double layer capacitance ( $C_{DL}$ ). A specific capacitance ( $C_s$ ) value  $C_s = 0.035 \text{ mF cm}^{-2}$  (0.5 M H<sub>2</sub>SO<sub>4</sub>) and  $C_s = 0.040 \text{ mF cm}^{-2}$  (1 M KOH) are adopted from previous reports.<sup>[2]</sup> As a result, the ECAS of Ni<sub>2</sub>P NPs/CC is calculated to be 149 and 184 using the following equation:

$$\text{ECAS} = C_{DL}/C_s$$

**5. Faradic efficiency.** The generated gas was confirmed by gas chromatographic (GC) analysis and measured quantitatively using a calibrated pressure sensor to monitor the pressure change in the cathode compartment of a H-type electrolytic cell. The FE was calculated by comparing the amount of measured oxygen generated by potentiostatic anodic electrolysis with calculated oxygen (assuming 100% FE). GC analysis was carried out on a GC-2014C (Shimadzu Co.) with thermal conductivity detector and nitrogen carrier gas. Pressure data during electrolysis were recorded using a CEM DT-8890 Differential Air Pressure Gauge Manometer Data Logger Meter Tester with a sampling interval of 1 point per second.

**5. Calculation of Turnover frequency (TOF):** Turnover frequency (TOF) is the best figure of merit with which to compare the activities of different catalyst materials. It is the number of H<sub>2</sub> molecules evolved per second per active site. For TOF calculations, the surface concentration of redox active sites associated with the redox Ni species should be first calculated, and the linear relationship between the oxidation peak current and scan rate is extracted from the electrochemical cyclic voltammetry scans. The slope of the line can be calculated based on the following equation:

$$\text{Slope} = n^2 F^2 A \Gamma_0 / 4RT$$

Where  $n$  is the number of electrons transferred;  $F$  is Faraday's constant;  $A$  is the surface area of the electrode;  $\Gamma_0$  is the surface concentration of redox active sites (mol

cm<sup>-2</sup>), and R and T are the ideal gas constant and the absolute temperature, respectively.<sup>[3]</sup> TOF values can be finally calculated from the formula:

$$\text{TOF} = \text{JA}/4\text{Fm}$$

Where TOF is based on the number of redox-active sites, J is the current density at a certain overpotential, A is the area of the electrode, 4 indicates the number of moles of electrons consumed for production of one mole of H<sub>2</sub> from water, F is Faraday's constant and m is the number of moles of active sites, m ( $m = A\Gamma_0$ ) (mol).<sup>[4]</sup>

### ICP-MS results

**Table S1.** Mass of nickel in the extracted solutions obtained with different extraction times.

Soaking time	1 h	2 h	4 h	8 h
Mass / mg	46.5 ± 3.4	100.6 ± 4.2	160.3 ± 6.8	210.4 ± 9.6

**Table S2.** Contents of nickel and other impurities in the extracted solution after 8 h extraction.

	Ni	Fe	Co	Cu	Ba	Ca
Mass / mg	210.4 ± 12.6	15.6 ± 2.2	5.15 ± 0.68	0.6 ± 0.1	0.5 ± 0.18	65.8 ± 7.6

**Table S3.** Contents of nickel and other impurities in the solution obtained by dissolving the deposited NiO.

	Ni	Fe	Co	Cu	Ba	Ca
Mass / mg	130.1 ± 8.6	–	–	–	–	–

### Monitoring of Ni(CO)<sub>4</sub> by miniature microplasma optical emission spectrometer and evaluation of the CVD efficiency

The generated Ni(CO)<sub>4</sub> is very toxic and thus its leakage should be monitored in-situ in real-time. Therefore, a miniature microplasma optical emission spectrometer (MP-OES) reported earlier<sup>[5]</sup> was connected to the CVD reactor to monitor the remaining Ni(CO)<sub>4</sub>, as shown in Figure S1. Briefly, the miniature MP-OES consists of an atmospheric-pressure point discharge (PD) and a commercial hand-held charge coupled device (CCD) spectrometer (Maya 2000 Pro, Ocean Optics Inc., Dunedin, FL98, USA) having a 0.4 nm spectral resolution and a usable spectral range from 200

to 600 nm. The PD was generated and sustained by connecting the two electrodes to a compact ac neon sign transformer power supply (NGB408BL, Electronic Equipment Factory of Jinshi, Guangzhou, China; 14 cm long  $\times$  6 cm wide  $\times$  5 cm high, with a rated output of 8 kV, 30 kHz, and 24 W at 220 V, 60 Hz input). The Ni(CO)<sub>4</sub> from the CVD reactor was excited in the PD and generated atomic emission lines of nickel (Figure S2), which were detected with the CCD spectrometer. In order to obtain high sensitivity and avoid interference from background, the Ni 231.6 nm line was used for quantification and monitoring. Figure S3 shows the real-time monitoring of Ni(CO)<sub>4</sub> from the CVD reactor. From this figure, we can conclude that almost of all the generated Ni(CO)<sub>4</sub> was decomposed and deposited on the substrate of CC while any leakage of Ni(CO)<sub>4</sub> could be effectively monitored.

The CVD efficiency of Ni(CO)<sub>4</sub> can be evaluated via the detection of the intensity of the specific atomic emission line of nickel before and after CVD. Similar to the conventional CVD techniques, the pyrolysis temperature significantly affects the CVD efficiency of Ni(CO)<sub>4</sub> and plays a key role in the synthesis of NiO NPs. Therefore, the effect of temperature on the CVD efficiency of Ni(CO)<sub>4</sub> was investigated, as shown in Figure S4. The results show that nickel response decreased with increasing deposition temperature, indicating that the CVD efficiency of Ni(CO)<sub>4</sub> on the CC substrate is improved as the temperature rises. When the temperature is above 160 °C, the response remains constant, consistent with the results of EDX (Figure S5i and S5l).

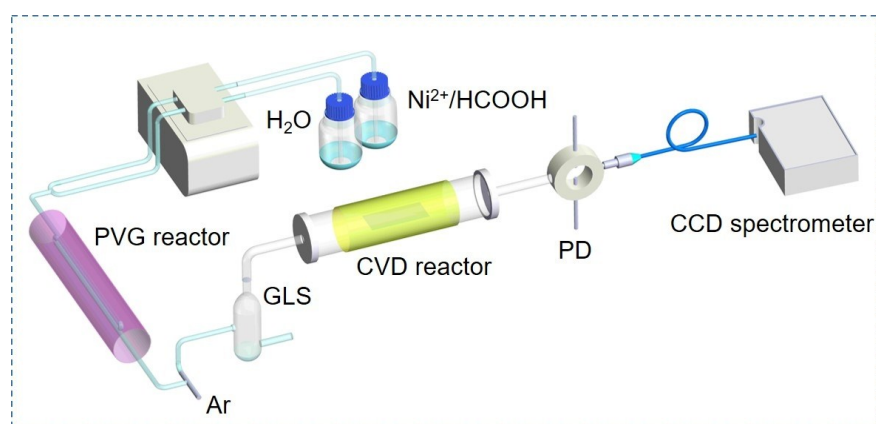


**Figure S1.** Schematic of measurement of Ni(CO)<sub>4</sub> using optical emission spectrometer.

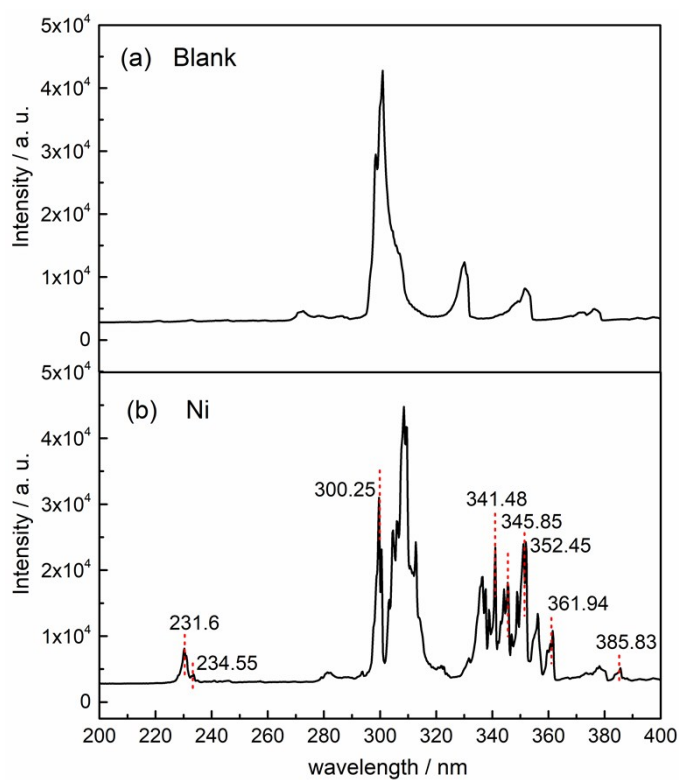


**Figure S2.** Atomic emission lines generated with PVG-PD-OES. (a) blank; (b) atomic emission line of Ni.

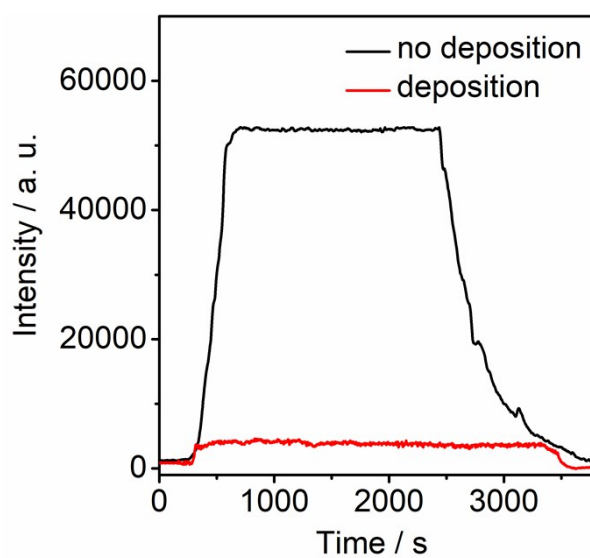


**Figure S3.** Real-time monitoring of nickel leakage during the deposition process.

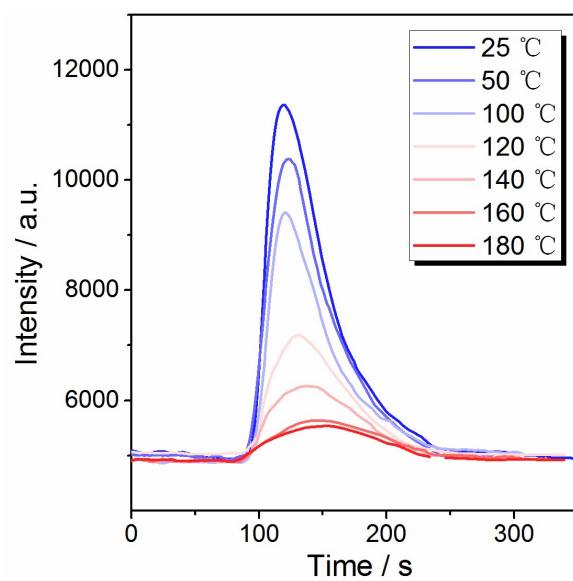


**Figure S4.** Atomic emission spectrum of Ni after deposition at various temperatures.

### **Characterization of Ni<sub>2</sub>P/CC synthesized at different deposition temperatures**

As shown in Figure S6, as-grown Ni<sub>2</sub>P NPs/CC at 160 °C provided a  $\eta_{10}$  of 69 and 73 mV in both acidic and alkaline solution, respectively, clearly superior to that at lower temperature, while a bit lower than that obtained using Ni<sub>2</sub>P prepared at 180 °C. This suggests that a 160 °C pyrolysis temperature is more suitable for the synthesis of Ni<sub>2</sub>P NPs/CC. The catalytic performance of Ni<sub>2</sub>P was also in agreement with the results of XRD wherein Ni<sub>2</sub>P with crystallization and spherical morphology can be obtained at 160 °C. Additionally, a series of materials (pyrolyzing at 100–180 °C) was characterized by SEM and EDX analysis (Figure S5), which demonstrated that the contents of Ni and P reach a relatively high ratio at temperatures above 160 °C. Thus, the excellent catalytic performance of Ni<sub>2</sub>P NPs/CC synthesized at 160 °C for HER in both acidic and alkaline media may be attributed to highly efficient deposition of Ni(CO)<sub>4</sub> at this temperature and complete with morphology maintained during the phosphorization of the as-synthesized NiO NPs/CC leading to a successful synthesis of Ni<sub>2</sub>P NPs/CC.

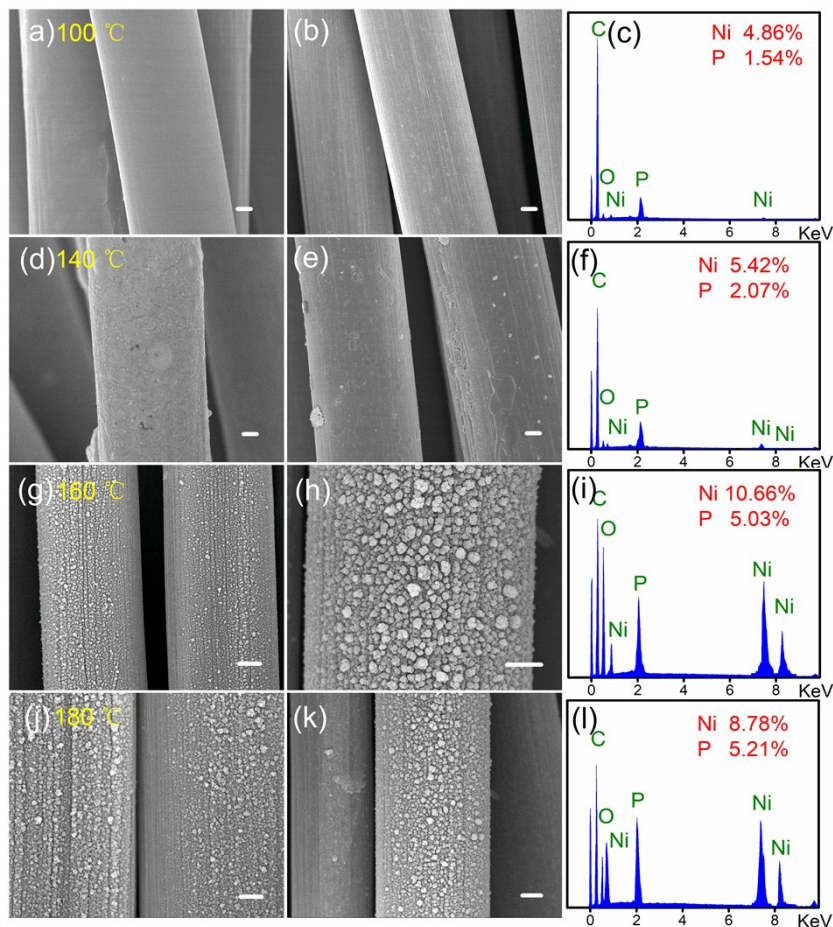


**Figure S5.** SEM of NiO NPs/CC (a) (d) (g) (j) and as-prepared Ni<sub>2</sub>P NPs/CC (b) (e) (h) (k) obtained by pyrolysis of Ni(CO)<sub>4</sub> at 100, 140, 160 and 180 °C. The EDS spectrum of Ni<sub>2</sub>P NPs/CC with corresponding temperature (c) (f) (i) (l). Scale bars in SEM image, 1  $\mu$ m.

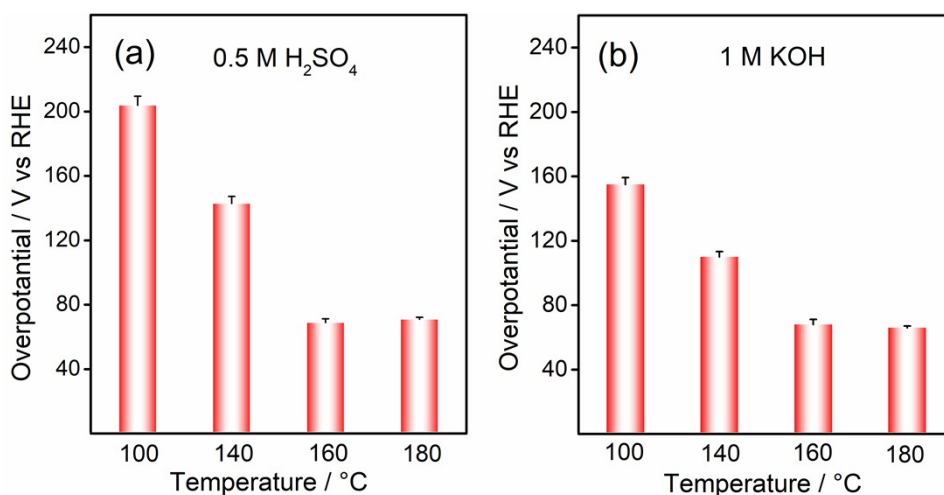


**Figure S6.** Comparison of electrocatalytic performance (as measured by the overpotential that the electrocatalyst needs to afford a current density of 10 mA cm<sup>-2</sup>) in 0.5 M H<sub>2</sub>SO<sub>4</sub> (a) and 1 M KOH (b) at 100, 140, 160 and 180 °C.

## Electrochemical measurements

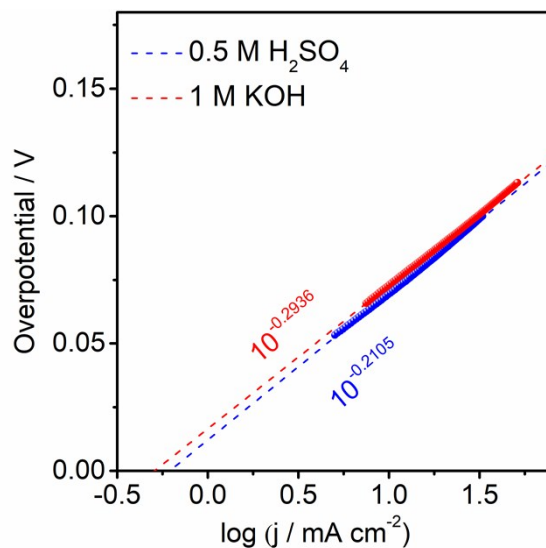


**Figure S7.** Exchange current density for HER of Ni<sub>2</sub>P NPs/CC in 0.5 M H<sub>2</sub>SO<sub>4</sub> and 1 M KOH aqueous solutions calculated from corresponding Tafel plots by an extrapolation method.

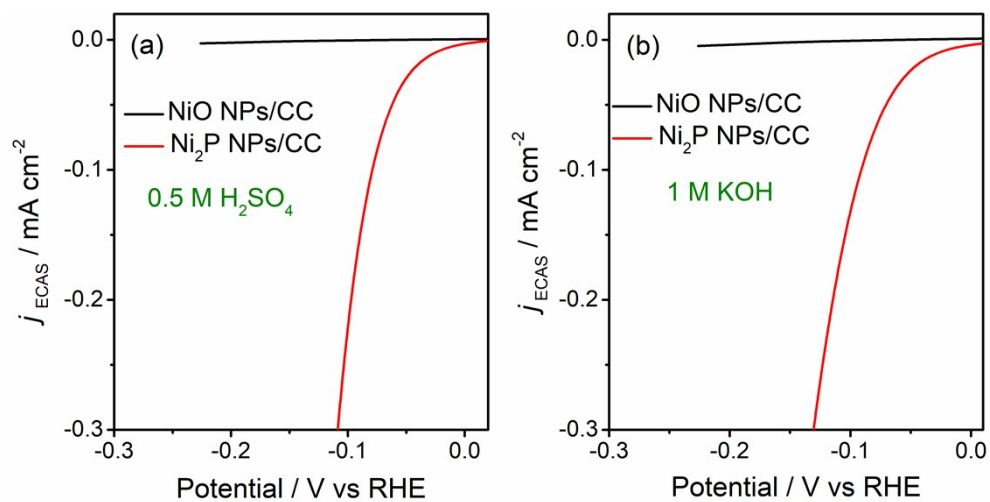


**Figure S8.** Polarization curves obtained with the NiO NPs and Ni<sub>2</sub>P NPs/CC in 0.5 H<sub>2</sub>SO<sub>4</sub> and 1 M KOH with iR compensation based on ECAS at a scan of 2 mV s<sup>-1</sup>.

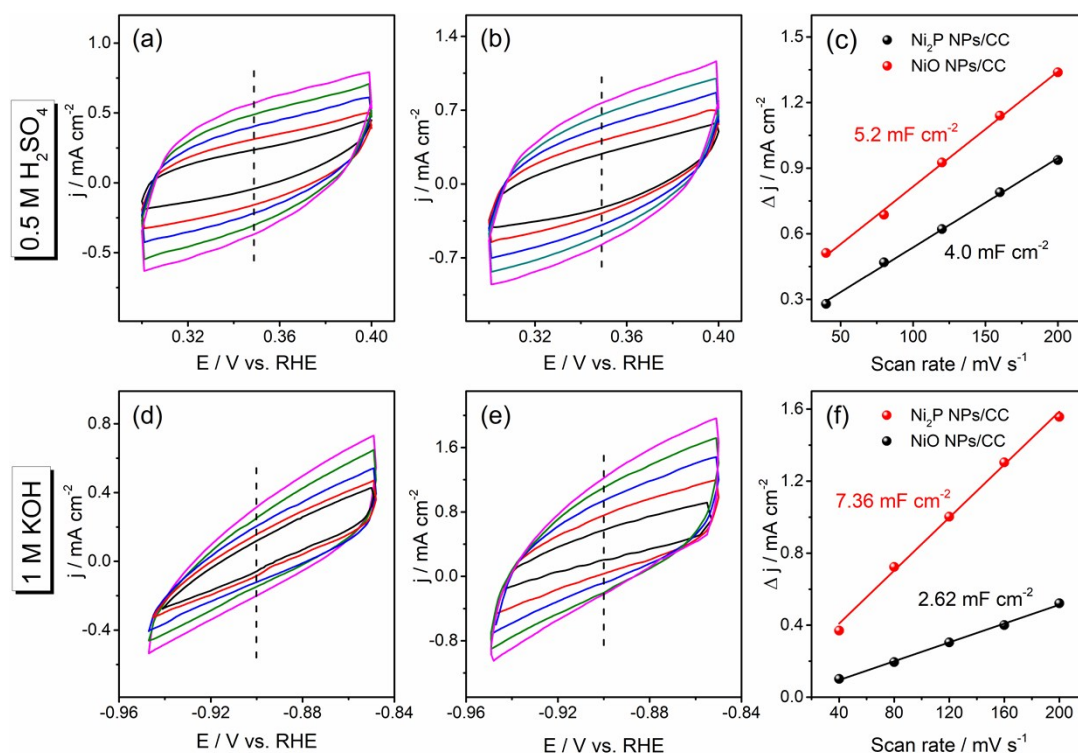


**Figure S9.** Cyclic voltammograms for (a) (d) NiO and (b) (e) Ni<sub>2</sub>P NPs/CC in the non-faradaic capacitance current range at scan rates of 40, 80, 120, 160 and 200 mV s<sup>-1</sup> in 0.5 M H<sub>2</sub>SO<sub>4</sub> and 1 M KOH. (c) (f) The capacitive currents at 0.35 V, 0.90 V as a function of scan rate for NiO and Ni<sub>2</sub>P NPs/CC in 0.5 M H<sub>2</sub>SO<sub>4</sub> and 1 M KOH.

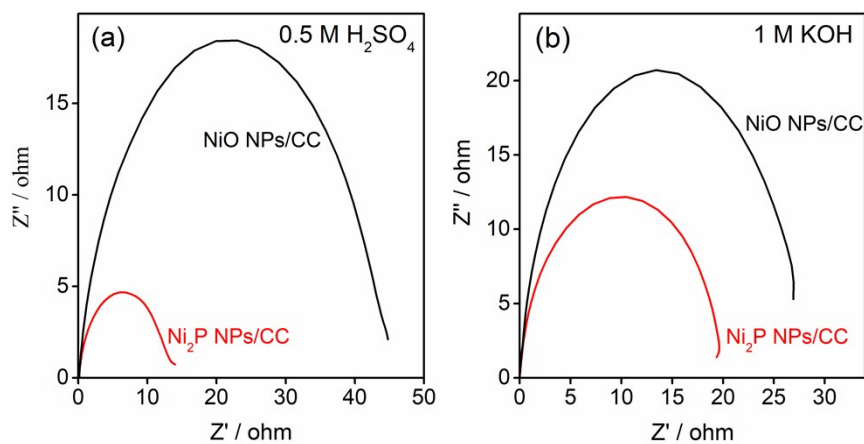


**Figure S10.** Nyquist plots of NiO and Ni<sub>2</sub>P NPs/CC in 0.5 M H<sub>2</sub>SO<sub>4</sub> (a) and 1 M KOH (b) at an overpotential of 50 mV.

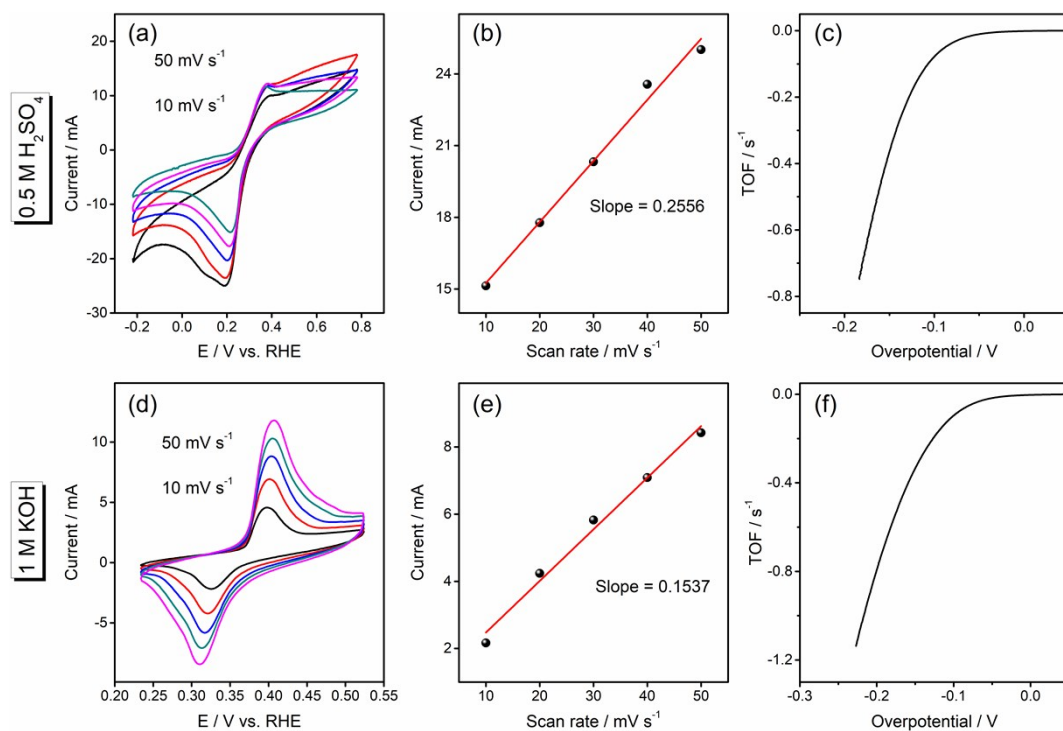


**Figure S11.** CVs of Ni<sub>2</sub>P NPs/CC at different scan rates increasing from 10 mV s<sup>-1</sup> to 50 mV s<sup>-1</sup> in (a) 0.5 M H<sub>2</sub>SO<sub>4</sub> and (d) 1 M KOH. Reduction peak current versus scan rate plots for Ni<sub>2</sub>P NPs/CC in (b) 0.5 M H<sub>2</sub>SO<sub>4</sub> and (e) 1 M KOH. Turnover frequency (TOF) at a constant overpotential in (c) 0.5 M H<sub>2</sub>SO<sub>4</sub> and (f) 1 M KOH.

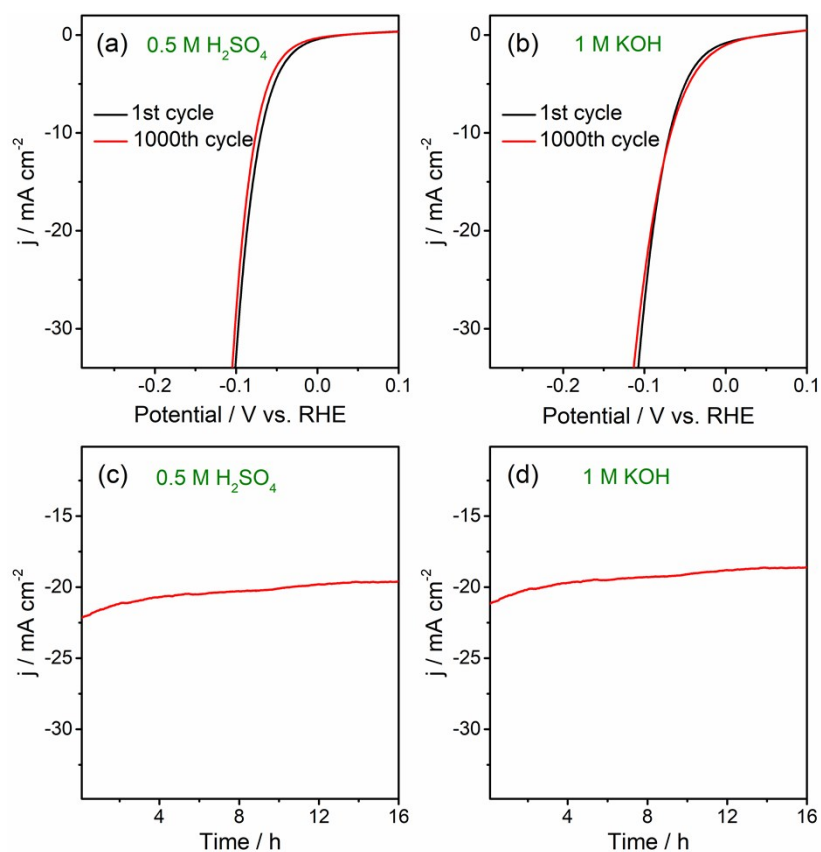


**Figure S12.** Polarization curves of Ni<sub>2</sub>P NPs/CC in both 0.5 M H<sub>2</sub>SO<sub>4</sub> (a) and 1 M KOH (b) initially and after 1000 CV between +0.1 and -0.3 V vs. RHE. Current-time (I-t) curve obtained for a hydrogen evolution reaction with Ni<sub>2</sub>P NPs/CC at -0.1V both in 0.5 M H<sub>2</sub>SO<sub>4</sub> (c) and 1 M KOH (d).

## Comparison of the electrocatalytic activities obtained by the proposed nickel-based phosphide electrocatalyst and other similar electrocatalysts

**Table S4.** Comparison of the electrocatalytic activity of recently reported nickel-based phosphide electrocatalysts under two media conditions.

Catalyst	Electrolyte	$\eta_{\text{onset}}$ (mV)	Loading (mg cm <sup>-2</sup> )	Tafel plot (mV dec <sup>-1</sup> )	Ref.
Ni <sub>2</sub> P	0.5 M H <sub>2</sub> SO <sub>4</sub>	69 @10 mA cm <sup>-2</sup>	10.8	55	This work
	1M KOH	73 @10 mA cm <sup>-2</sup>		73	
Ni <sub>2</sub> P@graphene	0.5 M H <sub>2</sub> SO <sub>4</sub>	98 @10 mA cm <sup>-2</sup>	1	56	6
NiP <sub>2</sub>	1 M KOH	148 @ 10 mA cm <sup>-2</sup>	~3.8	93.4	7
				-	
Carbon@Ni-P	0.5 M H <sub>2</sub> SO <sub>4</sub>	98 @10 mA cm <sup>-2</sup>	0.3	58.8	8
NiP	1M KOH	130 @10 mA cm <sup>-2</sup>	10.58	58.5	9
Ni <sub>5</sub> P <sub>4</sub> -Ni <sub>2</sub> P	0.5 M H <sub>2</sub> SO <sub>4</sub>	120 @10 mA cm <sup>-2</sup>	68.2	79.1	10
Ni <sub>5</sub> P <sub>4</sub> /Ni <sub>2</sub> P	1 M H <sub>2</sub> SO <sub>4</sub>	23/42 @10 mA cm <sup>-2</sup>	177	33/38	11
	1M KOH	49/69 @10 mA cm <sup>-2</sup>		98/118	
Ni <sub>2</sub> P	0.5 M H <sub>2</sub> SO <sub>4</sub>	120 @10 mA cm <sup>-2</sup>	3.5	68	12
	1M KOH	41 @~90 mA cm <sup>-2</sup>		50	
Ni <sub>5</sub> P <sub>4</sub>	0.5 M H <sub>2</sub> SO <sub>4</sub>	140 @ 10 mA cm <sup>-2</sup>	13.9	40	13
	1M KOH	155 @ 10 mA cm <sup>-2</sup>		53	
Ni <sub>2</sub> P	0.5 M H <sub>2</sub> SO <sub>4</sub>	75 @10 mA cm <sup>-2</sup>	4.3	51	14
	1M KOH	102 @10 mA cm <sup>-2</sup>		65	
Ni <sub>2</sub> P	1 M H <sub>2</sub> SO <sub>4</sub>	138 @20 mA cm <sup>-2</sup>	2.0	60	15
Ni <sub>2</sub> P	1 M H <sub>2</sub> SO <sub>4</sub>	140 @20 mA cm <sup>-2</sup>	0.38	87	16
	1M KOH	250 @20 mA cm <sup>-2</sup>			
Ni <sub>2</sub> P	0.5 M H <sub>2</sub> SO <sub>4</sub>	130 @20 mA cm <sup>-2</sup>	~1	46	17

## References

1. W. Zhou, X. Wu, X. Cao, X. Huang, C. Tan, J. Tian, J. Wang, H. Zhang, *Energy Environ. Sci.* 2013, **6**, 2921–2924.
2. D. Zhou, L. He, W. Zhu, X. Hou, K. Wang, G. Du, C. Zheng, X. Sun, A. M. Asiri, *J. Mater. Chem. A*, 2016, **4**, 10114–10117.
3. S. Pintado, S. Goberna-Ferrón, E. C. Escudero-Adán, J. R. Galán-Mascaós, *J. Am. Chem. Soc.* 2013, **135**, 13270–13273.

4. M. Gong, Y. Li, H. Wang, Y. Liang, J. Z. Wu, J. Zhou, J. Wang, T. Regier, F. Wei, H. Dai, *J. Am. Chem. Soc.* 2013, **135**, 8452–8455.
5. S. Zhang, H. Luo, M. Peng, Y. Tian, X. Hou, X. Jiang, C. Zheng, *Anal. Chem.* 2015, **87**, 10712–10718.
6. S. Jeoung, B. Seo, J. M. Hwang, S. H. Joo, H. R. Moon, *Mater. Chem. Front.* 2017, **1**, 973–978.
7. Z. Pu, Y. Xue, W. Li, I. S. Amiinu, S. Mu, *New J. Chem.* 2017, **41**, 2154–2159.
8. X. Wang, W. Li, D. Xiong, D. Y. Petrovykh, L. Liu, *Adv. Funct. Mater.* 2016, **26**, 4067–4077.
9. G. F. Chen, T. Y. Ma, Z. Q. Liu, N. Li, Y. Z. Su, K. Davey, S. Z. Qiao, *Adv. Funct. Mater.* 2016, **26**, 3314–3323.
10. X. Wang, Y. V. Kolen'ko, X.-Q. Bao, K. Kovnir, L. Liu, *Angew. Chem. Int. Ed.* 2015, **54**, 8188–8192.
11. A. B. Laursen, K. R. Patraju, M. J. Whitaker, M. Retuerto, T. Sarkar, N. Yao, K. V. Ramanujachary, M. Greenblatt, G. C. Dismukes, *Energy Environ. Sci.* 2015, **8**, 1027–1034.
12. Y. Shi, Y. Xu, S. Zhuo, J. Zhang, B. Zhang, *ACS Appl. Mater. Inter.* 2015, **7**, 2376–2384.
13. M. Ledendecker, S. Krick Calderón, C. Papp, H. P. Steinrück, M. Antonietti, M. Shalom, *Angew. Chem. Int. Ed.* 2015, **127**, 12538–12542.
14. P. Jiang, Q. Liu, X. Sun, *Nanoscale* 2014, **6**, 13440–13445.
15. Z. Pu, Q. Liu, C. Tang, A. M. Asiri, X. Sun, *Nanoscale* 2014, **6**, 11031–11034.
16. L. Feng, H. Vrubel, M. Bensimon, X. Hu, *Phys. Chem. Chem. Phys.* 2014, **16**, 5917–5921.
17. E. J. Popczun, J. R. McKone, C. G. Read, A. J. Biacchi, A. M. Wiltrout, N. S. Lewis, R. E. Schaak, *J. Am. Chem. Soc.* 2013, **135**, 9267–9270.